The Journal of Experimental Biology 200, 65–81 (1997)
Printed in Great Britain © The Company of Biologists Limited 1997
JEB0463

LOCOMOTOR DESIGN OF DOLPHIN VERTEBRAL COLUMNS: BENDING MECHANICS AND MORPHOLOGY OF *DELPHINUS DELPHIS*

JOHN H. LONG, JR[1,*], D. ANN PABST[2], WILLIAM R. SHEPHERD[1] AND WILLIAM A. MCLELLAN[2]

[1]*Department of Biology, Vassar College, Poughkeepsie, NY 12601, USA* and [2]*Department of Biological Sciences and Center for Marine Science Research, University of North Carolina at Wilmington, Wilmington, NC 28403, USA*

Accepted 19 September 1996

Summary

The primary skeletal structure used by dolphins to generate the dorsoventral bending characteristic of cetacean swimming is the vertebral column. In the vertebral column of the saddleback dolphin *Delphinus delphis*, we characterize the static and dynamic mechanical properties of the intervertebral joints, describe regional variation and dorsoventral asymmetries in mechanical performance, and investigate how the mechanical properties are correlated with vertebral morphologies. Using a bending machine that applies an external load (N m) to a single intervertebral segment, we measured the resulting angular deformation (rad) of the segment in both dorsal extension and ventral flexion. Intervertebral segments from the thoracic, lumbar and caudal regions of the vertebral column were tested from five individuals. Using quasi-static bending tests, we measured the initial (low-strain) bending stiffness (N m rad^{-1}) as a function of segment position, direction of bending (extension and flexion) and sequential cutting of intervertebral ligaments. We found that initial bending stiffness was significantly greater in the lumbar region than in adjacent thoracic and caudal regions, and all joints were stiffer in extension than in flexion. Cutting the interspinous ligaments significantly lowered the initial bending stiffness. Stiffness in extension is predicted (r^2=0.554) by the length and width of the intervertebral disc and the length of the cranial vertebral body in the segment. Stiffness in flexion is predicted (r^2=0.400) by the width of the nucleus pulposus, the length of the caudal vertebral body in the segment and the height of the transverse processes from the ventral surface of the vertebral body. We also performed dynamic bending tests on intervertebral segments from the lumbo-caudal joint and the joint between caudal vertebrae 7 and 8. Dynamic bending stiffness (N m rad^{-1}) increases with increasing bending amplitude and is independent of bending frequency. Damping coefficient (kg m^2 rad^{-2} s^{-1}) decreases with increasing bending amplitude and frequency. Resilience (% energy return) increases from approximately 20 % at low bending amplitudes (±0.6 °) to approximately 50 % at high bending amplitudes (±2.9 °). Based on these findings, the dolphin's vertebral column has the mechanical capacity to help control the body's locomotor reconfigurations, to store elastic energy and to dampen oscillations.

Key words: intervertebral discs, vertebrae, cetaceans, stiffness, damping, elastic energy, swimming, saddleback dolphin, *Delphinus delphis*.

Introduction

Dolphins swim by rhythmically bending a variably flexible beam – their vertebral column. With the evolution of fully aquatic swimming behavior, the vertebral column of cetaceans has undergone comprehensive changes in function and structure compared with that of the group's hypothesized terrestrial ancestors (Slijper, 1936). Recently, putative evolutionary intermediates have been unearthed, yielding, compared with terrestrial mammals, vertebral columns with reduced thoracic spinous processes, unfused and lengthened sacral vertebrae and robust lumbar neural spines (Thewissen *et al.* 1994; Gingerich *et al.* 1994). Thewissen *et al.* (1994) used these vertebral features to argue that early cetaceans swam in a manner similar to all extant representatives of the order – namely by dorsoventral bending of the axial skeleton. Yet we know little about the relationship of vertebral morphology – either skeletal or ligamentous – to the biomechanics of bending vertebral columns. The goal of the present study was to elucidate that relationship by examining the static and dynamic mechanical behaviors of intervertebral joint segments of the saddleback dolphin *Delphinus delphis.*

The vertebral column of cetaceans, as in all vertebrates, transmits forces that contribute to movement and that control the range and pattern of body deformations (e.g. Alexander *et al.* 1985; Bennett *et al.* 1987; Gal, 1992, 1993*a*; Hebrank, 1982; Hebrank *et al.* 1990; Long, 1992, 1995; Pabst, 1993; Slijper, 1936, 1946; Wainwright, 1983). These functions are

*e-mail: jolong@vassar.edu.

controlled, in part, by the morphologies and mechanical properties of the segments that form the vertebral column: the vertebrae and the ligaments that serially connect them. For example, Hebrank *et al.* (1990) demonstrated that the neural and hemal arches, zygopophyses and intervening ligaments stabilize the intervertebral joints of blue marlin (Pisces: *Makaira nigricans*) against axial compression and lateral shearing – functions critical to the mechanical integrity of the vertebral column. In mammalian vertebral columns, Gal (1993*b*) demonstrated that the relationship between vertebral structure and bending mechanics is species-specific. For example, resistance to ventral flexion is controlled primarily by the ligamenta flava in some monkeys and wallabies and by intervertebral discs in tigers and jaguars (Gal, 1993*b*).

Vertebral morphologies and bending mechanics also vary regionally and may be important in controlling the pattern of force transmission and deformation along the body axis. Precaudal intervertebral discs of blue marlin are less stiff than the caudal joints – the increased stiffness may accelerate the undulatory wave during swimming (Long, 1992). The lumbosacral joint in a number of terrestrial mammals is significantly less resistant to bending than the lumbar–lumbar joints, a regional specialization that may enhance pelvic limb movement (Gal, 1993*a*).

The extent of bending varies both along the length of the animal and in the up- and downstrokes of many cetaceans, as shown by kinematic analyses of swimming motions and qualitative bending tests (e.g. Videler and Kammermans, 1985; Wainwright *et al.* 1987). Bottlenose dolphins (*Tursiops truncatus*) and a number of other toothed cetaceans swim by oscillating the caudal third of their body (Fish, 1993). The small deformations cranial to the dorsal fin make body bending difficult to measure except at the atlanto-occiptial joint (Pabst, 1993). As determined by manually bending a carcass, harbor porpoises (*Phocoena phocoena*) appear to have two 'centers of rotation', one at the lumbo-caudal joint and the other at the caudal joint at the insertion of the fluke blades (Parry, 1949). Slijper (1946) suggested that the perceived increased resistance to bending in the lumbar region was due to the relatively large second moment of area of the vertebral bodies (a cross-sectional shape factor used in engineering beam theory). Regional variations in bending and dorsoventral asymmetries have also been attributed to the increased length of spinous processes, extra articulating processes (Slijper, 1946) and the ventral longitudinal ligament (Parry, 1949).

No quantitative analysis exists that tests the relationship between any morphological feature and the bending mechanics of the vertebral column in any cetacean species (although see Bennett *et al.* 1987 for the mechanical properties of the caudal vertebral column in the harbor porpoise). The goals of the present study are (1) to characterize the static and dynamic mechanical properties of the intervertebral joint segments in the saddleback dolphin, (2) to determine whether regional variation and/or dorsoventral asymmetries in mechanical performance exist, (3) to describe how the mechanical properties are correlated with vertebral morphology, and (4) to hypothesize functional roles of the vertebral column in a swimming dolphin.

Materials and methods

Animals and intervertebral joints

We investigated the vertebral columns of five saddleback dolphins, *Delphinus delphis* Linnaeus, at the United States National Museum (Table 1). These individuals were captured incidental to fishing operations in the north-west Atlantic Ocean, frozen immediately, and kept in that disposition until our dissections.

For bending tests, we removed single intervertebral joint segments from the backbone, each consisting of a cranial vertebra, an intact ligamentous joint and a caudal vertebra (Figs 1, 2A). These joint segments were bathed continuously in physiological saline (Pantin, 1964) as they thawed, warmed to room temperature and then underwent bending experiments. Eight joint segments were sampled from three regions of the

Table 1. *Saddleback dolphin (*Delphinus delphis*) specimens used in this study*

	571396 (USNM #)	571400 (USNM #)	571410 (USNM #)	571449 (USNM #)	NY 08/10/91 (field #)
Mass (kg)	137	138	149	Unknown	55.5
Length (m)	2.20	2.16	2.16	2.02	1.74
Sex	Male	Male	Male	Male	Female
Joints examined in static tests					
Intact	T4/5; C7/8; C13/14	T4/5–C13/14	All	T4/5–C20/21	T4/5–C13/14
Interspinous ligaments cut	T4/5; C7/8; C13/14	T4/5–C13/14	T4/5–C7/8	TL–C13/14	TL–C13/14
Intertransverse ligaments cut	C7/8	T4/5–C7/8	T4/5–C7/8	T4/5–LC; C13/14	T4/5–C13/14
Joints examined in dynamic tests	LC; C7/8	LC; C7/8	LC; C7/8	None	None

USNM # refers to the permanent identification number assigned by the United States National Museum. Field # refers to the initial collection number.

See Fig. 4 for explanation of the experimental treatments: intact, interspinous ligaments cut and intertransverse ligaments cut.

C, caudal; LC, lumbo-caudal; T, thoracic; TL, thoraco-lumbar; numbers refer to the axial positions of the cranial and caudal vertebrae, respectively. See Fig. 1 for further details.

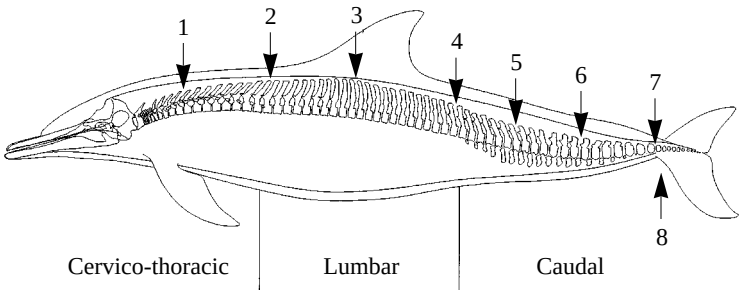

Fig. 1. Vertebral column of saddleback dolphin, *Delphinus delphis*. Left lateral view. The vertebral column has seven cervical, 13 thoracic, 22 lumbar and 31 caudal vertebrae (regions as defined by Rommel, 1990). Numbers indicate the intervertebral joints investigated: (1) thoracic 4/5, (2) thoraco-lumbar, (3) lumbar 10/11, (4) lumbo-caudal, (5) caudal 7/8, (6) caudal 13/14, (7) caudal 20/21 and (8) prefluke/fluke (caudal 21/22). Note that the ribs are not pictured.

backbone (Fig. 1): thoracic 4/5, thoraco-lumbar, lumbar 10/11, lumbo-caudal, caudal 7/8, caudal 13/14, caudal 20/21 and prefluke/fluke (where the two numbers, when used, refer to the axial positions of the cranial and caudal vertebrae, respectively). Prior to testing, joints were preconditioned for 5–10 bending cycles, after which the stiffness of the joints was repeatable within 10 % of the mean (see 'Bending tests' below).

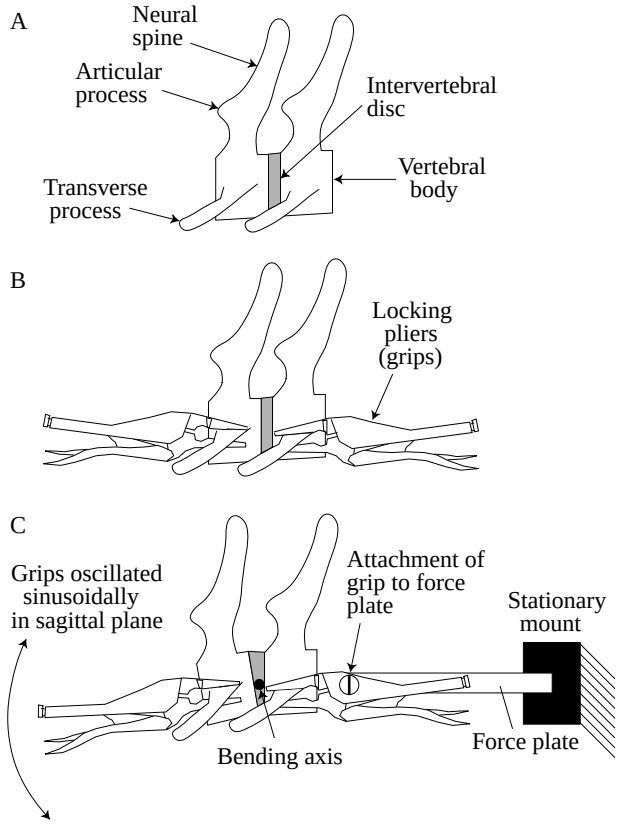

Fig. 2. Bending of a single intervertebral joint. Left lateral view. (A) Typical test segment. Of the several intervertebral ligaments normally present, only the intervertebral disc is shown here, for clarity. (B) Gripping the vertebrae. One pair of locking pliers was attached to each of the four transverse processes (only the left side is shown here). Pliers were positioned close to the vertebral body to avoid twisting the transverse processes. To prevent slippage, compression from the pliers was adjusted until no movement could be detected visually between the grips and the transverse processes at the highest bending amplitudes. (C) Dorsoventral bending in the sagittal plane. Grips on one vertebra were oscillated sinusoidally in extension and flexion; grips on the other vertebra were held stationary by their attachment to the force plate (see Fig. 3 for details of bending machine).

Bending machine

To measure their mechanical properties, intervertebral segments were bent in a machine (Fig. 3), modified from Long (1992), which applied an angular strain (θ, rad) and measured the resulting bending moment (M, N m). To grip the segment, needle-nose locking pliers (Sears Craftsman) were secured to each of the four transverse processes of the two vertebrae close to the vertebral bodies; the bending moment was applied to the joint *via* these bony processes (see Fig. 2). The pliers, in turn, were mounted onto the machine so that the intervertebral segment was bent in the dorsoventral plane, with the axis of bending passing through the dorsoventral and rostro–caudal midpoint of the intervertebral disc (Fig. 3). The moment arm on the stationary side of the machine was kept constant for all joints and tests. The arrangement was visually inspected during preconditioning to ensure that there was no slippage between the pliers and the transverse processes.

For quasi-static bending tests, the bending moment was applied manually to the intervertebral joint *via* the input linkage (Fig. 3). Joints were bent in dorsal extension and ventral flexion. The bending moment was measured using a half-bridge foil strain gauge (120 Ω) configuration with each gauge glued onto either side of an aluminum bar. The gauges were excited by a bridge amplifier (Omega Engineering, model DMD-520). The angular displacement, θ, caused by the bending moment was monitored by a rotary-variable differential transducer (Schaevitz, model R30D). Voltage outputs from both transducers were digitally sampled (100 Hz) using an analog-to-digital converter (National Instruments, model NB-MIO-16L) and a microcomputer (Apple Macintosh, model IIcx).

For dynamic bending tests, the input linkage of the machine was attached to a motor in such a way as to produce a reciprocating, sinusoidal motion (Fig. 3). The bending frequency (Hz) was determined by selecting the rotational speed of the shunt-wound d.c. motor using an electronic controller (Minark Electric, model SL52). The maximal bending amplitude, θ_0, was controlled by altering the length of the input linkage (the distance between pivots *A* and *D* in Fig. 3).

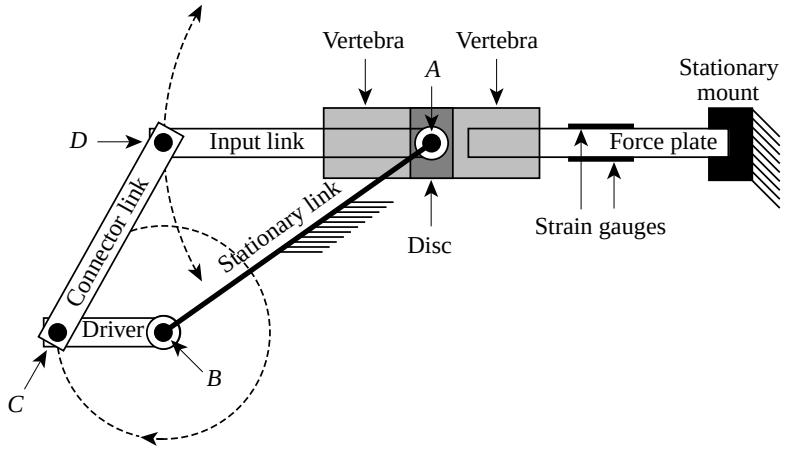

Fig. 3. Bending machine consisting of a motorized four-bar linkage and cantilevered force plate. Pivots between linkages are labeled *A–D*. Reciprocating sinusoidal motion at pivot *D* (dashed arc) was driven by a motor (not shown) at pivot *B* that rotated pivot *C* through a circular path (dashed circle). Pivots *A* and *B* remained stationary. The bending motion (rad) was measured by a rotary variable differential transducer (RVDT) colinear with the shaft of pivot *A*. The bending moment (N m) caused by the motion was measured by two 120 Ω foil strain gauges mounted on a cantilevered force plate of aluminum stock (16.0 cm×5.5 cm×0.7 cm, length × height × width). The moment arm (the distance from *A* to the strain gauges) was kept constant for all tests. Each intervertebral segment was rigidly mounted *via* its associated vertebrae to the force plate and the input link (see Fig. 2 for details of specimen gripping), with the intervertebral disc centered at the axis of rotation, pivot *A*. The bending amplitude was adjusted by changing the distance between pivots *A* and *D*.

Mechanical properties

Using load and displacement information from the transducers, we calculated the bending stiffness, damping coefficient and resilience. Bending stiffness, k (N m rad^{-1}), is the instantaneous slope of the line relating the externally applied bending moment, M, and the resulting angular displacement, θ:

$$k = \frac{dM}{d\theta} . \quad (1)$$

For the quasi-static tests, stiffness was measured as the initial stiffness when the joint was first bent in either dorsal extension or ventral flexion. In this initial region, stiffness was always linear up to 0.01 rad and there was no neutral (zero stiffness) zone.

Under dynamic (time-dependent) external loads, the Newtonian equation of motion for a single-degree-of-freedom system was used to calculate the dynamic stiffness, k, and the damping coefficient, c (kg m^2 rad^{-2} s^{-1}) (Den Hartog, 1956):

$$M = [k\theta_0\sin(\omega t - \delta)] + [c\omega\theta_0\cos(\omega t - \delta)] - [I\omega^2\theta_0\sin(\omega t - \delta)] , \quad (2)$$

where the first term on the right-hand side of the equation is the stiffness moment, the second term is the damping moment, the third term is the moment due to angular acceleration of the mass (inertia), θ_0 (rad) is the amplitude of the angular displacement, ω (rad s^{-1}) is the angular frequency, t (s) is time, δ (rad) is the phase lag between the bending moment and the angular displacement, and I (kg m^2 rad^{-3}) is the moment of inertia (also see Long, 1992). The bending stiffness, k, the damping coefficient, c, and the phase lag, δ, are the mechanical properties that determine the relationship between a sinusoidally imposed bending moment, M, and the resulting sinusoidal motion. The inertial term was dropped from our calculations because the bending moment was measured on the stationary side of the machine, where accelerations were small enough to be negligible (see Fig. 3). Because the stiffness and damping moments are 90° out of phase (sine and cosine functions, respectively), for any given values of θ and ω, k was determined from the value of M and δ at the time, t, when the damping term was zero. Likewise, c was determined at the time, t, when the stiffness term was zero. Note that this equation of motion assumes that k and c are constant with respect to θ and ω; values of k and c at given values of θ and ω are therefore averages over that specific range of motion that underestimate the corresponding instantaneous values. The equation of motion was used, instead of the loss and storage moduli commonly used in biomechanics (see Wainwright *et al.* 1976), because it makes no assumptions about the organization and arrangement of the material and structure of the intervertebral joint.

The stiffness, k, and damping coefficient, c, determine the phase lag, δ, in the following manner (Denny, 1988):

$$\tan\delta = \frac{c\omega}{k - I\omega^2} . \quad (3)$$

tanδ, in turn, determines the resilience, R (%), the proportion of energy returned by the elastic components of the structure over a complete bending cycle (Wainwright *et al.* 1976):

$$R = \frac{100}{e^{\pi\tan\delta}} . \quad (4)$$

The resilience of each joint at the various values of θ and ω was calculated by substituting the measured value for δ into equation 4.

Bending tests

Quasi-static bending tests were performed to measure the stiffness of the initial, or low-strain, response of the intervertebral joint. Initial stiffness, the slope of the loading curve (equation 1), provides a simple diagnostic of the bending resistance offered by the intervertebral segments as a function of the following independent variables: (1) region of the backbone (thoracic, lumbar, caudal, fluke), (2) direction of

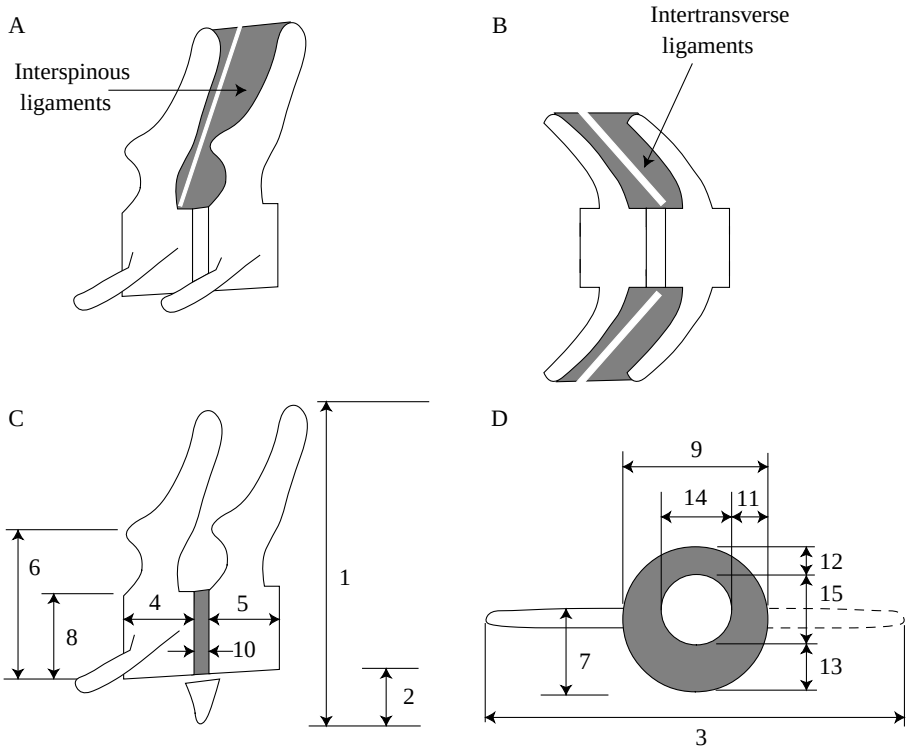

Fig. 4. Intervertebral and vertebral morphology. (A,B) Cuts (white bars) made to intervertebral ligaments. Treatments were performed sequentially from A to B to determine the relative contribution of each ligament to initial bending stiffness. (A) First cut: interspinous ligaments cut, left lateral view. (B) Second cut: intertransverse ligaments cut, ventral view. Both left and right ligaments cut. (C,D) Morphometric measurements of structural features of vertebrae and intervertebral ligaments, left lateral and cranial view, respectively. These aspects of morphology were chosen because of their direct relationship to size, shape and potential mechanical contribution predicted from beam theory (see Denny, 1988): (1) vertebral segment height, (2) chevron height, (3) transverse process width, (4) cranial vertebral body length, (5) caudal vertebral body length, (6) articular process height, (7) transverse process height, (8) intervertebral disc height, (9) intervertebral disc width, (10) intervertebral disc length, (11) annulous fibrosus width, (12) annulous fibrosus dorsal height, (13) annulous fibrosus ventral height, (14) nucleus pulposus width and (15) nucleus pulposus height. For measurements, see Table 2.

bending (extension, flexion) and (3) integrity of intervertebral ligaments (see Fig. 4A,B). The starting position of the joint chosen as zero displacement and moment was the position assumed by the mounted joint following a single displacement of the free end (pivot *D*, Fig. 3) of the input linkage; the resulting resonance of the joint produced angular oscillations about a reproducible position that we defined as the 'straight' or 0° angular postion. Reproducibility of this position was possible since the joints lacked neutral zones. It is unknown how this *in vitro* straight posture relates to the posture of the spine *in vivo*.

Each intervertebral segment was tested in the following order: intact (quasi-static), intact dynamic, interspinous ligaments cut (quasi-static) and intertransverse ligaments cut (quasi-static). The total elapsed time, from the first to the last test, ranged from 13 to 17 min. Note that owing to operational errors during some tests, not all joints are represented throughout the testing sequence (see Table 1); this uneven sampling is responsible, in some cases, for small apparent increases (less than 13%) in initial stiffness following the cutting of ligaments (see Results). To account for possible changes in the material properties over the course of the experiment and for investigator error, we performed a repeatability analysis consisting of three separate quasi-static tests of an intact joint tested over 15 min (the average duration of the battery of tests); the joints were bathed with saline throughout and analyzed by three separate investigators. For time-dependent effects on material properties, no consistent directional changes in stiffness were detected between trials, and values varied by ±5% (1 S.D., N=3) about the mean stiffness. To determine the magnitude of investigator error, three separate investigators independently analyzed the same data; the stiffness values from the three varied by ±6% (1 S.D., N=3) about the mean. When the between-trials and between-investigator effects were combined, the stiffness values varied by ±10% (1 S.D., N=9) about the mean.

For two individual dolphins (571449 and NY 08/10/91; see Table 1), we video-taped the joints as they underwent bending tests. Markers on the vertebrae were digitized through time (for digitizing methods, see McHenry *et al.* 1995), allowing us to measure the position of the segment's rotational axis and to monitor the overlap of the articular process of the caudal vertebral body with the neural spine of the cranial vertebral body.

Dynamic bending tests were performed to measure dynamic mechanical properties and their dependence on angular deformation and angular frequency (see equations 2–4). To assess frequency-dependence, intervertebral joints were bent at bending frequencies of 0.5–5 Hz at 0.5 Hz increments (angular frequencies, ω, of π–10π rad s^{-1}). This range of bending frequencies was chosen to encompass the tailbeat frequencies (0.75–3 Hz) measured in live, steadily swimming bottlenose dolphins (Fish, 1993). It should be noted that the bottlenose dolphins were larger than the saddleback dolphins used in this study (2.61 m *versus* 2.06 m mean total length, respectively; Table 1); as a result, we may expect tailbeat frequencies in live saddleback dolphins to exceed 3 Hz. To assess strain-dependence, intervertebral joints were bent at five amplitudes:

0.012, 0.019, 0.026, 0.033 and 0.049 rad (0.6–2.9 °). This range of testing amplitudes was chosen to encompass the maximal intervertebral strains (2 °) calculated from a sustained locomotor sequence of a bottlenose dolphin (Pabst, 1993). It should be noted that tailbeat amplitude remains constant over a range of steady swimming speeds (Fish, 1993) and may increase during accelerations (Pabst, 1993). Because most of this motion is limited to the caudal tailstock, we measured dynamic properties only in the lumbo-caudal and caudal 7/8 segments. For each bending amplitude, intervertebral segments were bent over the entire range of bending frequencies.

Morphometrics

To determine whether regional variation in vertebral morphology corresponded to regional variation in bending stiffness, we measured 15 linear characteristics of the vertebrae and intervertebral ligaments of all test segments (Fig. 4C,D; Table 2). These features were chosen because of their presumed mechanical importance in bending (see Discussion).

Statistical analyses

For quasi-static and dynamic bending tests, the dependence of stiffness, damping coefficient and resilience on the independent variables was determined using analysis of variance (ANOVA) (SAS Institute, 1985). Because we repeatedly measured mechanical properties from a single joint, and from many joints within an individual dolphin, we

Table 2. *Morphometric measurements of the structural features of vertebrae and intervertebral discs*

Structural feature	Thoracic 4/5	Thoraco-lumbar	Lumbar 10/11	Lumbo-caudal	Caudal 7/8	Caudal 13/14
Vertebral segment height	10.17 (±1.451)	14.35 (±1.242)	14.91 (±1.520)	13.19 (±1.391)	11.34 (±1.619)	9.11 (±1.237)
Chevron height	–	–	–	–	5.46 (±0.750)	3.88 (±0.466)
Transverse process width	9.35 (±0.800)	21.32 (±1.314)	18.82 (±1.350)	15.30 (±0.758)	13.28 (±0.719)	7.36 (±2.355)
Cranial vertebral body length	2.47 (±0.195)	3.00 (±0.244)	2.27 (±0.200)	2.24 (±0.238)	2.61 (±0.295)	3.08 (±0.387)
Caudal vertebral body length	2.69 (±0.224)	2.90 (±0.269)	2.25 (±0.199)	2.29 (±0.284)	2.65 (±0.331)	3.22 (±0.425)
Articular process height	5.45 (±0.639)	6.93 (±0.728)	7.63 (±1.184)	8.32 (±1.261)	8.07 (±0.841)	7.21 (±1.626)
Transverse process height	5.34 (±0.359)	2.58 (±0.321)	2.46 (±0.277)	2.54 (±0.505)	2.63 (±0.523)	2.59 (±0.353)
Intervertebral disc height	2.90 (±0.290)	3.45 (±0.274)	3.77 (±0.250)	3.98 (±0.244)	4.03 (±0.290)	4.02 (±0.174)
Intervertebral disc width	3.10 (±0.151)	3.49 (±0.305)	3.89 (±0.232)	4.02 (±0.298)	4.23 (±0.252)	4.07 (±0.198)
Intervertebral disc length	0.65 (±0.107)	0.55 (±0.073)	0.56 (±0.066)	0.53 (±0.052)	0.68 (±0.122)	0.87 (±0.108)
Annulous fibrosus width	0.74 (±0.085)	0.89 (±0.200)	0.99 (±0.134)	0.95 (±0.115)	0.97 (±0.175)	0.98 (±0.079)
Annulous fibrosus dorsal height	0.64 (±0.131)	0.80 (±0.066)	0.91 (±0.145)	0.91 (±0.142)	1.08 (±0.125)	0.96 (±0.206)
Annulous fibrosus ventral height	0.85 (±0.084)	0.97 (±0.152)	1.10 (±0.077)	1.05 (±0.151)	0.86 (±0.136)	0.89 (±0.171)
Nucleus pulposus width	1.41 (±0.179)	1.66 (±0.426)	1.71 (±0.289)	2.18 (±0.240)	2.00 (±0.372)	2.01 (±0.274)
Nucleus pulposus height	1.38 (±0.175)	1.54 (±0.213)	1.71 (±0.168)	2.01 (±0.130)	1.96 (±0.306)	2.14 (±0.405)

Values are means (±S.D.) from five dolphins (see Table 1). All values are in cm.
For definitions of the structural features, see Fig. 4.
For positions of vertebrae, see Fig. 1.

treated 'individual' as a factor (see Tables 3 and 7) that behaves like a randomized block effect without replication (Sokal and Rohlf, 1981). This removes the effects of differences between individuals from the other factors. For the quasi-static tests, main factors were individual, bending direction ('direction' in Table 3), structural disposition before and after cutting of ligaments ('structure'), and axial joint position ('joint'). In addition, interaction terms were also considered. Planned contrasts were run between categories within the structure and joint variables. For the dynamic tests, main factors were individual, joint, amplitude ('amplitude' in Table 7) and frequency ('frequency'). Interaction terms were also considered. Planned contrasts were run within the amplitude and frequency variables. For correlations between morphological features and initial bending stiffness, we performed a stepwise linear regression to determine which morphological features were the best predictors (Wilkinson, 1989). We also measured the correlations among structural features using Pearson coefficients (r) and the Bonferroni procedure to correct for multiple comparisons (Wilkinson, 1989). For all analyses, the significance level was 0.05. Missing values are detailed in Table 1.

Results

Initial bending stiffness

Quasi-static bending stiffness of the intervertebral ligaments varies regionally (Fig. 5; Tables 3, 4). In both extension and flexion, bending stiffness is greatest at the lumbo-caudal joint, with decreasing stiffness towards the head and tail. There are no significant differences between either thoracic 4/5 and thoraco-lumbar joint segments or caudal 7/8 and caudal 13/14 joint segments (Table 4). Initial stiffness is greater in extension than in flexion throughout the column (Table 3).

Cutting the interspinous ligaments significantly reduces the initial stiffness of the joints (Fig. 5; Tables 3, 4). Cutting the intertransverse ligaments has no detectable effect on stiffness. The interaction terms in the ANOVA are not significant (Table 3).

Vertebral motion as recorded on video tape showed that in all cases (two individuals, six joint positions, three structure treatments each) the joints were rotating about the intervertebral disc. Overlap of the articular processes of the neural spine of the caudal vertebra with the neural spine of the cranial vertebra, at low initial bending strains, was clearly seen in the intact and cut segments of thoracic 4/5, thoraco-lumbar, lumbo-caudal and caudal 7/8 (see also Fig. 1). The cranial

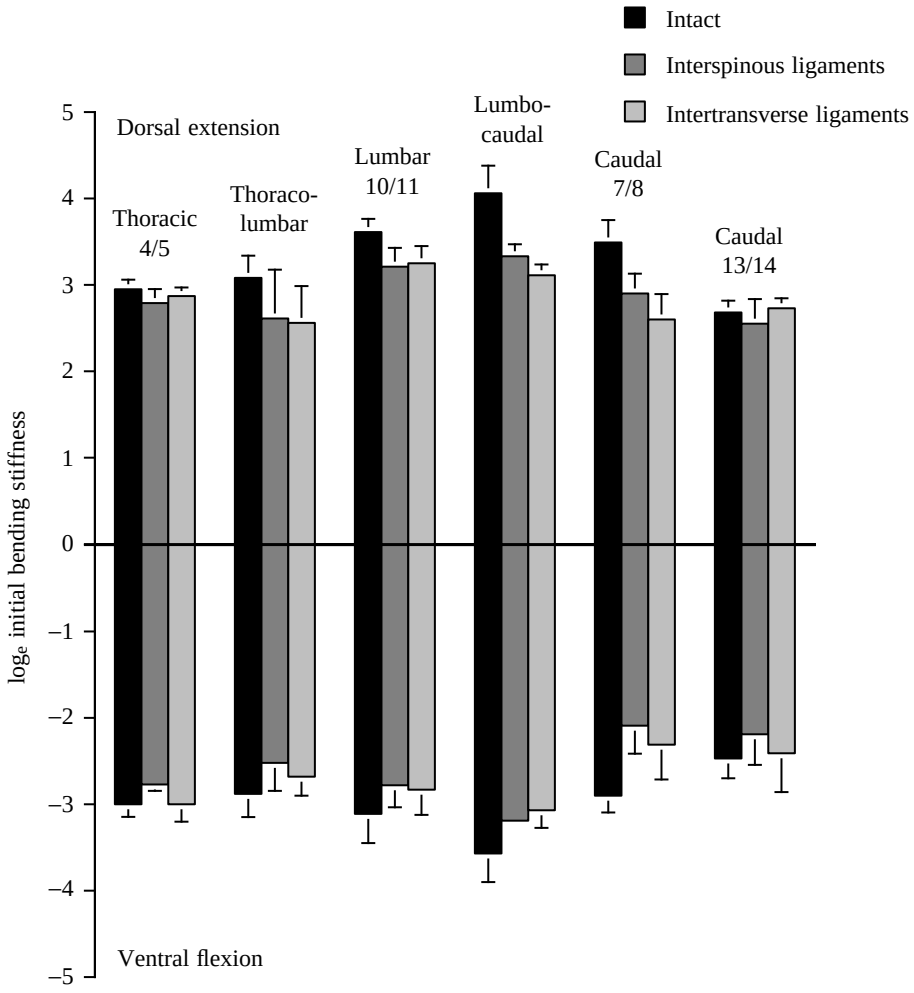

Fig. 5. Initial bending stiffness (N m rad^{-1}) of intervertebral joints. Bars are means (±S.E.M.) of stiffness by joint position, bending direction and structural integrity of the ligaments. These main effects are all significant (Table 3). In comparisons between adjacent joints, stiffness increases significantly from the thoraco-lumbar to lumbar 10/11 and from the lumbar 10/11 to lumbo-caudal joints (Table 4). Stiffness decreases significantly from the lumbo-caudal to caudal 7/8 joint. The joints are stiffer in extension than they are in flexion. Cutting the interspinous ligaments significantly decreases the bending stiffness, while cutting the intertransverse ligaments has no effect. Non-significant increases in the mean stiffness of the joints following the final ligament cutting in eight of the 12 cases is caused by missing values for some individuals and by variation in repeatability (for further explanation, see Materials and methods and Table 1).

Table 3. *Quasi-static bending stiffness of dolphin intervertebral joints*

Factor	*F*	*P*
Individual (4)	8.23	0.0001
Direction (1)	9.98	0.0020
Structure (2)	12.14	0.0001
Joint (5)	10.70	0.0001
Direction × Structure (2)	0.50	0.6058
Direction × Joint (5)	1.44	0.2154
Structure × Joint (10)	0.88	0.5567
Direction × Structure × Joint (10)	0.18	0.9974

Degrees of freedom (d.f.) are given in parentheses to the right of each factor; error d.f. were 110.

Sample size was 150 (not including 30 missing cells; see Table 1).

The factor 'Individual' was treated as a randomized block effect without replication; therefore, no interaction term using that factor could be run. Factors are considered significant when $P<0.05$.

Summary of *F* values (Type III sums of squares) from ANOVA with bending stiffness as the dependent variable. Values of bending stiffness were $\log_e$-transformed to normalize the distribution of the variable. Results from the transformed analyses are given here. Untransformed data yielded similar qualitative results.

Table 4. *Comparisons of quasi-static bending stiffness of dolphin intervertebral joints within main effects*

Contrast	*F*	*P*
Intact *versus* interspinous ligaments (1)	17.73	0.0001
Interspinous ligament *versus* transverse (1)	0.02	0.8903
Thoracic 4/5 *versus* thoraco-lumbar (1)	3.53	0.0628
Thoraco-lumbar *versus* lumbar 10/11 (1)	8.68	0.0039
Lumbar 10/11 *versus* lumbo-caudal (1)	5.54	0.0204
Lumbo-caudal *versus* caudal 7/8 (1)	23.01	0.0001
Caudal 7/8 *versus* caudal 13/14	3.74	0.0557

Degrees of freedom (d.f.) are given in parentheses to the right of each factor; error d.f. for the entire model were 110 (see Table 3). Contrasts are considered significant when $P<0.05$.

The dashed line demarcates contrasts for the independent variables intervertebral structure (upper) and intervertebral joint position (lower).

Summary of *F* values (Type III sums of squares) from planned contrasts in ANOVA with bending stiffness as the dependent variable. Values of bending stiffness were $\log_e$-transformed to normalize the distribution of the variable. Results from the transformed analyses are given here. Untransformed data yielded similar qualitative results.

neural spine of lumbar joint 10/11 showed movement of tissue during extension and flexion indicative of articular process overlap. No bony overlap was detected during cutting of the ligaments; it is possible, however, that a cartilaginous articular process is present on the intact caudal neural spine. No articular process overlap was detected for caudal joint 13/14. It is important to note that we did not detect bone-to-bone contact during the low-amplitude strains associated with the range of bending motions used in the measurement of initial stiffness.

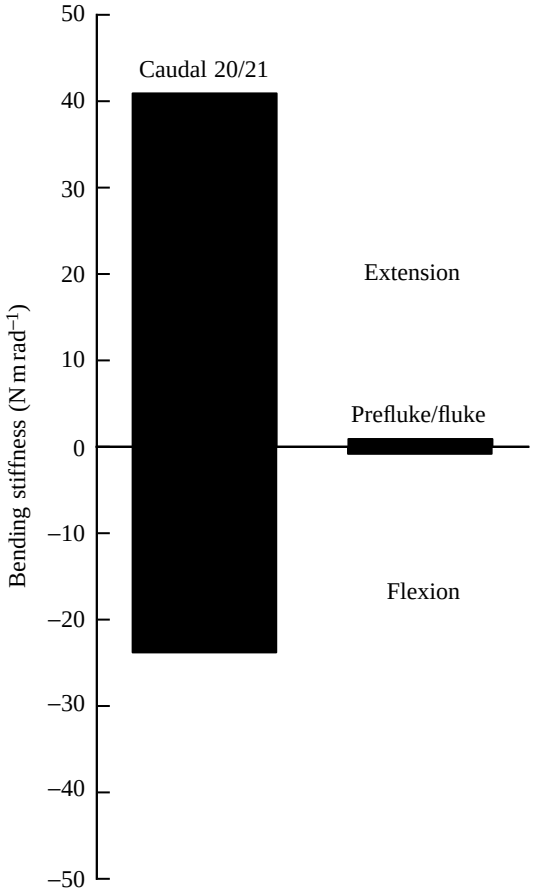

Fig. 6. Transition in bending stiffness from caudal tailstock to fluke. The initial bending stiffness of the caudal 20/21 joint is the mean from two individuals (see Table 1). The initial bending stiffness of the prefluke/fluke joint is the value from only one of those two individuals. The change in stiffness appears to be abrupt. Because of the low sample size, statistical tests could not be conducted (hence the lack of error bars).

While the sample size for the caudal 20/21 and prefluke/fluke joints does not permit statistical analysis (N=2 and 1, respectively; see Table 1), the most abrupt change in initial stiffness in the entire vertebral column, from approximately 25 N m rad^{-1} to less than 1 N m rad^{-1}, was seen in these two neighboring joints (Fig. 6).

Bending stiffness and vertebral morphology

Using stepwise linear regression, six of the 14 morphometric variables (Table 2) are significantly correlated with initial bending stiffness in extension and flexion (Table 5). 55 % of the variation in initial stiffness during extension (r^2=0.554) is predicted by the length and width of the intervertebral disc and the length of the cranial vertebral body in the segment (see Fig. 4 for morphology). 40 % of the variation in initial stiffness (r^2=0.400) during flexion is predicted by the width of the nucleus pulposus, the length of the caudal vertebral body in the segment and the height of the transverse processes.

Other structural features are correlated with these structural

Table 5. *Structural predictors of quasi-static, initial intervertebral bending stiffness*

Variable	Coefficient	S.E.M.	S.C.	T	r^2
Dorsal extension					
Disc length	–1.716	0.710	–0.392	–2.416 (0.0237)	
Disc width	0.791	0.208	0.539	3.807 (0.0009)	
Cranial vertebral body length	–0.556	0.258	–0.359	–2.153 (0.0415)	
					0.554 (0.0002)
Ventral flexion					
Nucleus pulposus width	0.708	0.298	0.426	2.375 (0.0259)	
Caudal vertebral body length	–0.843	0.230	–0.605	–3.662 (0.0012)	
Transverse process height	0.179	0.095	0.340	1.876 (0.0729)	
					0.400 (0.0058)

Bending stiffness values (Nm rad^{-1}) were log$_e$-transformed to normalize the variable's distribution.

Constants for the extension and flexion equations are 2.854 and 3.372, respectively.

P values are indicated in parentheses to the right of each value of T and r^2; only significant variables and overall models are returned in stepwise regression.

S.C., standardized coefficient.

Sample size was 28 (five individuals with six joints, each minus two missing values).

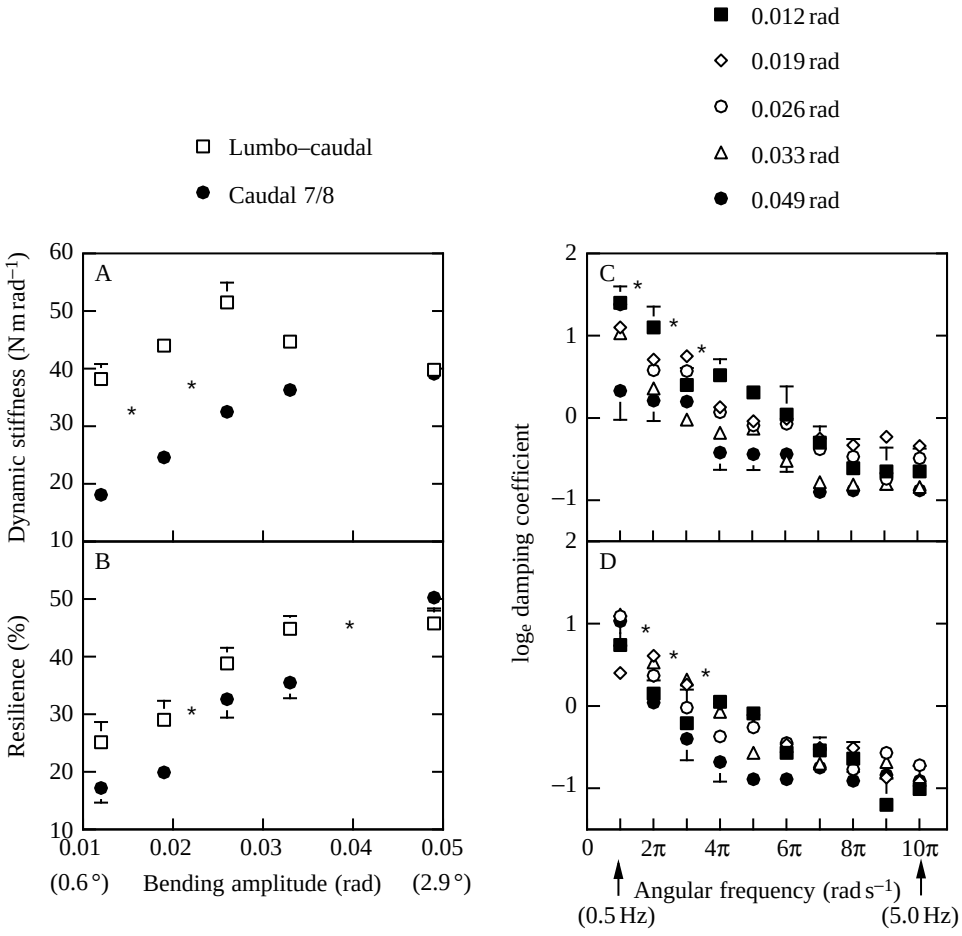

Fig. 7. Dynamic mechanical properties of the lumbo-caudal and caudal 7/8 joints. (A) In both joints, dynamic stiffness increases significantly from an amplitude of 0.012 to 0.026 rad (see Table 7). The lumbo-caudal joint was significantly stiffer than the caudal 7/8 joint. No significant frequency effects were detected. Values are means (±1 S.E.M.) from three individuals and 10 bending frequencies (N=30). (B) In both joints, resilience (% energy return) increases significantly from an amplitude of 0.019 to 0.026 rad and again from an amplitude of 0.033 to 0.049 rad. The lumbo-caudal joint was significantly more resilient than the caudal 7/8 joint. No significant frequency effects were detected. Values are as in A. (C) Damping coefficient (kg m^{-2} rad^{-2} s^{-1}) in the lumbo-caudal joint decreases significantly with increasing bending amplitude (from 0.026 to 0.049 rad) and frequency (from π to 4π rad s^{-1}). Points are means (±1 S.E.M.) from the same three individuals (N=3). (D) Damping coefficient in the caudal 7/8 joint follows the same pattern with respect to amplitude and frequency as that seen in the lumbo-caudal joint. The lumbo-caudal joint has a significantly greater damping coefficient. Asterisks denote significant differences between adjacent amplitudes or frequencies as determined in planned contrasts (ANOVA).

predictors of initial bending stiffness (Table 6). Correlation analysis of all pairwise combinations of the 14 features yields the following significant relationships after correction for multiple comparisons using the Bonferroni procedure: (1) length of the intervertebral disc is negatively correlated with vertebral segment height (r=–0.622) and transverse process width (r=–0.653), (2) width of the intervertebral disc is positively correlated with articular process height (r=0.737),

Table 6. *Correlations among vertebral and intervertebral structural features*

	Vertebral segment height	Transverse process width	Cranial vertebral body length	Caudal vertebral body length	Articular process height	Transverse process height	Inter-vertebral disc height	Inter-vertebral disc width	Inter-vertebral disc length	Annulous fibrosus width	Annulous fibrosus dorsal height	Annulous fibrosus ventral height	Nucleus pulposus width	Nucleus pulposus height
Vertebral segment height	*													
Transverse process width	**0.881**	*												
Cranial vertebral body length	–0.088	–0.118	*											
Caudal vertebral body length	–0.245	–0.321	**0.946**	*										
Articular process height	0.436	0.277	0.127	0.107	*									
Transverse process height	–0.299	–0.412	–0.001	0.186	–0.430	*								
Intervertebral disc height	0.259	0.089	0.226	0.177	**0.795**	**–0.611**	*							
Intervertebral disc width	0.163	0.031	0.171	0.117	**0.737**	–0.572	**0.919**	*						
Intervertebral disc length	**–0.622**	**–0.653**	0.484	0.547	–0.013	0.042	0.131	0.211	*					
Annulous fibrosus width	0.162	0.132	–0.036	–0.073	0.342	–0.580	0.428	0.425	0.135	*				
Annulous fibrosus dorsal height	0.050	0.039	0.113	0.117	**0.765**	–0.475	**0.650**	**0.661**	0.295	0.400	*			
Annulous fibrosus ventral height	0.482	0.362	–0.17	–0.244	0.290	–0.275	0.182	0.045	–0.261	0.429	0.012	*		
Nucleus pulposus width	0.034	–0.028	0.157	0.115	0.498	–0.338	**0.678**	**0.716**	–0.009	–0.123	0.402	–0.130	*	
Nucleus pulposus height	0.033	–0.133	0.181	0.164	0.466	–0.418	**0.811**	**0.812**	0.189	0.228	0.425	–0.202	**0.745**	*

Values are Pearson correlation coefficients (N=30, five individuals and six vertebral positions).
Coefficients in bold type are statistically significant (P<0.05) after correction for multiple comparisons using Bonferroni procedure.

Table 7. *Dynamic bending properties of dolphin intervertebral joints*

Factor	Stiffness	Damping	Resilience
Individual (2)	4.41 (0.0133)	8.21 (0.0004)	4.78 (0.0094)
Joint (1)	113.41 (0.0001)	30.23 (0.0001)	9.52 (0.0023)
Amplitude (4)	16.02 (0.0001)	12.63 (0.0001)	29.58 (0.0001)
Frequency (9)	0.30 (0.9747)	69.70 (0.0000)	1.63 (0.1084)
Joint × Amplitude (4)	9.29 (0.0001)	4.60 (0.0014)	2.02 (0.0935)
Joint × Frequency (9)	0.21 (0.9932)	0.58 (0.8117)	0.51 (0.8666)
Amplitude × Frequency (36)	0.12 (1.0000)	0.88 (0.6705)	0.55 (0.9837)
Joint × Amplitude × Frequency (36)	0.16 (1.0000)	0.77 (0.8271)	0.49 (0.9937)

P values are indicated in parentheses to the right of each value of *F*.

Degrees of freedom (d.f.) are given in parentheses to the right of each factor; error d.f. were 198.

Total sample size was 300 (three individuals, two positions, 10 frequencies, five amplitudes).

The factor 'Individual' was treated as a randomized block effect without replication; therefore, no interaction term using that factor could be run.

Summary of *F* values (Type III sums of squares) from ANOVAs performed separately on stiffness, damping coefficient and resilience. Values of damping coefficient were $\log_e$-transformed to normalize the distribution of the variable. Results from the transformed analyses are given here. Untransformed data yielded similar qualitative results.

intervertebral disc height (r=0.919), annulus fibrosus dorsal height (r=0.661), nucleus pulposus width (r=0.716) and nucleus pulposus height (r=0.812), (3) length of the cranial vertebral body is positively correlated with the length of the caudal vertebral body (r=0.946), (4) width of the nucleus pulposus is positively correlated with intervertebral disc height (r=0.678) and intervertebral disc width (r=0.716) and (5) height of the transverse processes is negatively correlated with intervertebral disc height (r=–0.611).

Dynamic mechanical properties

When measured over a range of amplitudes and frequencies (θ_0 and ω, respectively, in equation 2), dynamic bending stiffness in the lumbo-caudal and caudal 7/8 joints varies as a function of amplitude only, increasing from 0.012 to 0.026 rad and remaining statistically constant at higher amplitudes (Table 7; Fig. 7A). In addition, the lumbo-caudal joint is significantly stiffer than the caudal 7/8 over the entire range of amplitudes (Table 7). Resilience also increases only with amplitude, increasing from an amplitude of 0.019 to 0.026 rad and then again from an amplitudes of 0.033 to 0.049 rad (Table 7; Fig. 7B). In addition, the lumbo-caudal joint has significantly greater resilience than does the caudal 7/8 joint over the entire range of amplitudes (Table 7).

When measured over a range of amplitudes and frequencies (see equation 2), the damping coefficient in the lumbo-caudal and caudal 7/8 joints decreases significantly with increasing bending frequency and increasing bending amplitude (Table 7; Fig. 7C,D). Damping coefficient decreases significantly only until an angular frequency of 4π rad s^{-1} (2 Hz) is reached (Fig. 7C,D) and only begins to decrease with increasing bending amplitude at an amplitude of 0.026 rad.

Discussion

Using mechanical tests, this study is the first to test the hypotheses that the bending stiffness of the dolphin's vertebral column varies (1) with anatomical region, (2) with amplitude and frequency of joint motion and (3) with specific vertebral and intervertebral structures. We focus our discussion on these results and compare dolphin vertebral function with that of other aquatic vertebrates and terrestrial mammals.

Variation by region

In dorsoventral bending, the intervertebral joints of the saddleback dolphin are stiff near the middle of the body (i.e. the lumbo-caudal joint) and become more flexible towards the head and the tail (Fig. 5). The intervertebral joint at the base of the flukes is dramatically less stiff than any other joint tested in this study (Fig. 6).

Although, to the best of our knowledge, there are no kinematic data for swimming saddleback dolphins, the variation in the mechanical properties of their caudal vertebral column is consistent with variation in swimming motions measured from other species of odontocete cetaceans. For example, bottlenose dolphins swim by oscillating the caudal one-third of their bodies (Fish, 1993), where the caudal vertebral column displays decreased intervertebral joint stiffness compared with the lumbo-caudal joint (Fig. 5). During swimming in bottlenose dolphins, thrust is generated throughout the tailbeat cycle by continuously pitching the high-aspect-ratio fluke blades as they oscillate dorsoventrally (Fish, 1993). Mechanical results from our study suggest that the intervertebral joint at the base of the flukes acts like a low-resistance hinge, permitting subtle and continuous alterations of the angle of attack of the flukes.

Unlike the caudal tailstock, the thoracic region of bottlenose dolphins undergoes no measurable bending during steady swimming (Pabst, 1993). Mechanical results for saddleback dolphins, however, demonstrate that the thoracic and caudal intervertebral joints have similar stiffnesses (Fig. 5; Table 4). This lack of correspondence between intervertebral joint

stiffness and observed regional mobility during swimming may be due to the removal of the ribs prior to mechanical testing. We hypothesize that the ribcage provides considerable bending resistance *in vivo* although, to our knowledge, this has not been tested.

The regional pattern of intervertebral joint stiffness is also consistent with the hypothesis that axial muscles anchored in the lumbar spine cause extension of the caudal tailstock (Pabst, 1993). The lumbo-caudal joint has the greatest initial bending stiffness, which suggests that it has the resistance to serve as a region of insertion for the robust epaxial (upstroke) muscles.

Interestingly, the only epaxial muscle to insert onto the caudal vertebrae in the fluke, the m. extensor caudae lateralis, has the smallest force-generating capacity of any axial muscle. Pabst (1993) hypothesized that the movements of the flukes relative to the caudal tailstock must therefore be caused either by large hydrodynamic forces if the joint was stiff or by the smaller force available from the m. extensor caudae lateralis if the joint was flexible. The very low stiffness of the prefluke/fluke intervertebral joint suggests that the small forces generated by the m. extensor caudae lateralis may be sufficient to change or influence the angle of attack of the caudal fluke blades at times during the swimming cycle when hydrodynamic loads are small.

Intervertebral joint stiffness changes gradually along the length of the dolphin vertebral column (see Fig. 5; Table 4), except at the fluke vertebra, where there is a rather dramatic increase in joint compliance (Fig. 6). A similar pattern is seen at the lumbo-sacral joint of many terrestrial mammals (reviewed by Gal, 1993*a*). The lumbo-sacral joint has a large neutral zone (range of unloaded or unforced motion) and probably functions as a low-resistance joint to increase the range of movement of the pelvic girdle and hindlimb (Gal, 1993*a*).

The highly compliant fluke joint of dolphins and lumbo-sacral joint of terrestrial mammals are juxtaposed to joints of much higher stiffness. Thus, each intervertebral joint, as one in a series of discrete constructional units, represents an evolutionary ‘opportunity’ to modulate local mechanical behaviors along a continuous beam. Interestingly, we identified no morphological features of the caudal 20/21 *versus* prefluke/fluke vertebrae that would have allowed us to predict such abrupt differences in bending stiffness at the flukes (see below).

How does the regional pattern of intervertebral joint stiffness displayed in dolphins compare with that observed in other swimming vertebrates? Unlike dolphins, the caudal intervertebral joints of blue marlin are stiffer than the precaudal joints; the increased stiffness may increase the speed at which the undulatory propulsive wave travels down the body (Long, 1992). Similarly, in fish models, decreasing stiffness is associated with a decrease in the speed of the propulsive wave and a decrease in swimming speed (McHenry *et al.* 1995). Unlike undulatory swimming in fishes, dolphins are thunniform swimmers that do not use a traveling wave of bending to generate thrust. Thus, in dolphins, it is likely that

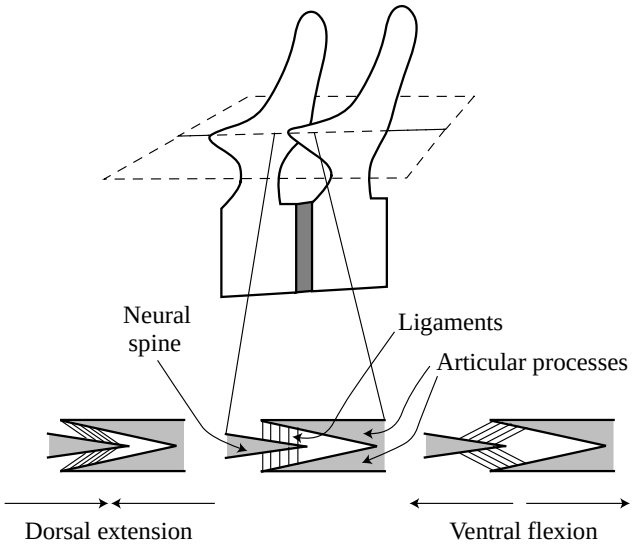

Fig. 8. Articular-process-stiffening mechanism. We propose that ligaments connecting the medial surfaces of the articular processes (caudal vertebra) to the lateral surface of the neural spine (cranial vertebra) are placed in tension during both extension and flexion. The top diagram is a left lateral view of a vertebral pair; the dashed and obliquely oriented plane is the frontal section through the articular processes shown below. This mechanism is consistent with the observation that removal of the interspinous ligaments decreases initial stiffness in both bending directions.

stiffness functions in one of several other ways: (1) to provide localized resistance to bending (origin *versus* insertion) and (2) to decelerate the tail at the end of the stroke (resistance proportional to angular displacement). In powered flight, birds use their major flight muscles to accelerate and decelerate the wings (Dial, 1992). A stiff vertebral column might provide, without muscular input, the same function.

Variation with structure

Dolphin intervertebral joints are stiffer in extension than they are in flexion (Fig. 5; Table 3). This is also true for a variety of terrestrial mammals, where the resistance to extension is caused by the touching of the articular facets of adjacent vertebrae (e.g. Gal, 1993*b*; Tencer *et al.* 1982). However, articular processes with opposing facets occur only in the cervical and cranial thoracic region in the vertebral column of bottlenose dolphins (Rommel, 1990). Thus, some other additional structural feature(s) must contribute to the stiffness in extension in the saddleback dolphin’s vertebral column (Fig. 5).

Resistance to both extension and flexion is dependent upon the integrity of the interspinous ligament (Fig. 5; Tables 3, 4). Resistance to extension is also positively correlated with width of the intervertebral disc and negatively correlated with the length of the intervertebral disc and length of the cranial vertebral body (r^2=0.554). Resistance to flexion is positively correlated with the width of the nucleus pulposus and the height of the transverse process, and negatively correlated with

the length of the caudal vertebral body (r^2=0.400). These predictive structural features are also correlated with other vertebral and intervertebral features (Table 6).

How do these structures directly affect bending stiffness? We would predict, using simple beam mechanics (see Den Hartog, 1949; Wainwright *et al.* 1976; Denny, 1988), that the interspinous ligament would increase resistance to flexion by providing tensile structures distal to the axis of bending at the intervertebral disc (e.g. Slijper, 1946; Gal, 1993*b*). It is more difficult to understand how this ligament influences joint stiffness in extension, since connective tissue fibers forming the ligament would presumably slacken as the neural spines moved closer together. However, because our video tapes showed overlap of the articular processes of the caudal vertebrae with the neural spine of the cranial vertebrae in at least four of the six joint positions (see Results), we propose that a novel structural mechanism exists for the purpose of stiffening the joint in both extension and flexion (Fig. 8). This articular-process-stiffening mechanism works by placing ligaments in tension during both extension and flexion. As the articular processes of the caudal vertebra shear past the neural spine of the cranial vertebra, medio–laterally oriented ligaments are lengthened. The ligamentous anatomy of this proposed mechanism remains to be confirmed.

In addition, structural predictors of bending stiffness (Table 5) may be understood by examining their correlations with other structures (Table 6). For example, the correlation of increasing nucleus pulposus width with increasing stiffness in flexion is at first puzzling (Table 5); however, the dimensions of the nucleus pulposus width are positively correlated, in turn, with two other cross-sectional disc features: disc height and disc width (Table 6). Together, this correlated set of features increases with increasing bending stiffness in a manner consistent with beam theory (Denny, 1988). Using these and other statistically significant associations, we have designed two hypothetical vertebral segments, one flexible (lowest stiffness) and one stiff (highest stiffness) (Fig. 9). These hypothetical designs are amalgams of features from the vertebral segments examined with statistical sample sizes (Table 2, between thoracic 4/5 and caudal 13/14). The design for a flexible segment is characterized by a long intervertebral joint and vertebral body, short neural spines and lateral processes and a small-diameter intervertebral disc. The design for a stiff segment is characterized by a short intervertebral joint and vertebral body, long neural spines and lateral processes, and a large-diameter intervertebral disc. Flexible segments minimize stiffness with a long intervertebral disc, as would be predicted from beam theory, where deformation of a structure under a constant external load is proportional to the cube of the length of the structure (Denny, 1988). The small

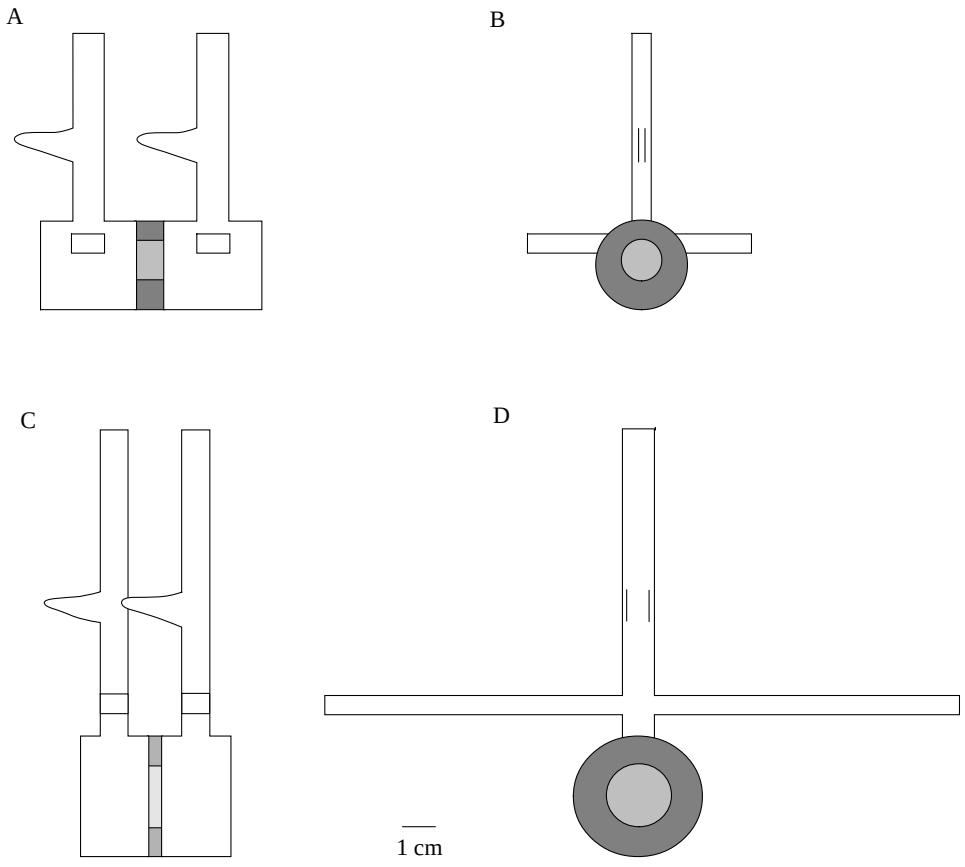

Fig. 9. Hypothetical design for flexible and stiff vertebral segments. Relative dimensions of bony and ligamentous structures are based on the results of stepwise regression (Table 5) and correlation analysis (Table 6). Minimal and maximal dimensions are taken from the dimensions of the six vertebral segments measured and tested (Table 2). (A) Left lateral view of a flexible (low stiffness) vertebral segment. This segment has long vertebral bodies and intervertebral disc, short neural spines and the transverse processes are located on the vertebral body. Note that the articular processes do not overlap the cranial neural spine. (B**)** Flexible vertebral segment from cranial view. Note the short transverse processes and the small diameter of the intervertebral disc and the nucleus pulposus. (C) Left lateral view of a stiff vertebral segment. This segment has short vertebral bodies and intervertebral disc, long neural spines and the transverse processes are located on the neural spine. Note that the articular processes overlap adjacent neural spines, a condition that allows the engagement of the articular-process-stiffening mechanism (see Fig. 8). (D) Stiff vertebral segment from cranial view. Note the long transverse processes and the large diameter of the intervertebral disc and the nucleus pulposus.

cross-sectional area of flexible segments further lowers the second moment of area of the structure, which is proportional to the flexural stiffness (Denny, 1988). The short neural spines also lower the overall second moment of area of the cross section of intervertebral ligaments. Finally, the long centra keep the articular processes on the neural spine from overlapping, thus inactivating the articular-process-stiffening mechanism described in the previous section. To understand the design of the stiff segments, these arguments are simply reversed. It is important to note that we do not understand the relationship between the length of the transverse processes, their vertical position and the segment's bending stiffness. Transverse processes may serve other functions that are correlated with, but not causally related to, the bending mechanics of the vertebral segments.

These results underscore the view that the functional relationship between bending stiffness and vertebral anatomy is complex and species-specific (e.g. Gal, 1993*a*, *b*; Long, 1992; Parry, 1949; Shirazi-Adl, 1989; Slijper, 1946; Tencer *et al.* 1982). Soft tissues, such as the interspinous ligaments, determine, in part, the bending stiffness of the vertebral segments in saddleback dolphins. Furthermore, only a fraction of the variation in bending stiffness is predicted by skeletal features alone (Table 5). Thus, any attempt to infer changes in locomotor function, and hence evolutionary transformations, from skeletons alone must be undertaken cautiously.

Variation with motion

The stiffness, resilience and damping behaviors of dolphin caudal intervertebral joints vary with bending amplitude (Fig. 7; Table 7). Intervertebral joint stiffness and resilience increase and damping coefficient decreases with increased bending amplitude. These patterns suggest that the dolphin caudal vertebral column is a stiff, moderately resilient beam when undergoing maximal bending. Although bottlenose dolphins do not appear to modulate tailbeat amplitude with increasing speeds during steady swimming (Fish, 1993), they do use maximal tail bending when accelerating from a near stop to speeds of approximately $2\,m\,s^{-1}$ (Wainwright *et al.* 1987; Pabst, 1993). Thus, amplitude-dependent mechanical behaviors of intervertebral joints may be more important during non-steady, accelerative swimming than during steady swimming in dolphins.

Another important feature of the intervertebral joints that may be determined from their dynamic mechanical properties is the total power required to bend a segment at different amplitudes and frequencies. Since mechanical power, the rate of working, is the product of force and velocity, the instantaneous bending power may be calculated as the product of bending moment and angular velocity. The power, P_s, required by an external load to overcome the stiffness, or displacement-proportional, component of the joint's resistance to bending is the product of the stiffness moment (see equation 2) and the angular velocity:

$$P_s = (k\theta_0 \sin\omega t)(\omega\theta_0 \cos\omega t)\,. \quad (5)$$

The power, P_d, required by an external load to overcome the damping, or velocity-proportional, component of the joint's resistance to bending is the product of the damping moment (see equation 2) and the angular velocity:

$$P_d = (c\omega\theta_0 \cos\omega t)(\omega\theta_0 \cos\omega t)\,. \quad (6)$$

The total instantaneous power required to overcome the mechanical resistance of the joint is the sum of P_s and P_d. Since stiffness, k, and damping coefficient, c, change with bending amplitude and frequency (Fig. 7), the dynamic mechanical behavior of the vertebral segments varies non-linearly in ways that may alter the backbone's functions during different swimming behaviors (Fig. 10). Several results are noteworthy in the caudal 7/8 joint segment. First, maximal total power varies over three orders of magnitude from a minimum of 0.003 W (θ=0.01 rad, $\omega=\pi\,rad\,s^{-1}$ or 0.5 Hz) to a maximum of 2.0 W (θ=0.05 rad, $\omega=10\pi\,rad\,s^{-1}$ or 5.0 Hz). Second, the greatest resilience (lowest relative damping) is seen at the highest amplitude and lowest frequency (θ=0.05 rad, $\omega=\pi\,rad\,s^{-1}$). Third, the lowest resilience is seen at the lowest amplitude and highest frequency (θ=0.01 rad, $\omega=10\pi\,rad\,s^{-1}$).

While measuring dynamic mechanical properties of elastic structures of the caudal tailstock at deformation frequencies of 2.2 Hz in *Lagenorhynchus obliquidens*, Bennett *et al.* (1987) and Blickhan and Cheng (1994) chose to ignore the bending properties of the vertebral column because of its low energy storage. That the maximal power required to bend a joint in our experiments varies over three orders of magnitude suggests that there may be circumstances in which the elastic properties of the vertebral column play a role in the mechanics of swimming. For example, at a bending amplitude of 0.05 rad (2.9 °) and a frequency of $10\pi\,rad\,s^{-1}$ (5.0 Hz), caudal joint 7/8 achieves its maximal stiffness power relative to other amplitudes and frequencies (Fig. 10). Since the area under the power–time curve represents the mechanical work, the positive work under the stiffness–power curve represents the total energy available to power recoil. Since the cycle period is 0.2 s, and the time to bend the joint maximally is one-quarter of that period, integration of equation 5 from 0 to 0.05 s yields 0.05 J of elastic energy stored in the joint. If there are 20 joints in the caudal tailstock (see Fig. 1), and assuming for the moment that they are all identical, then a total of 1.0 J of elastic energy is available to help power the unbending of the body and thrust production. In the best case, where none of this energy is lost (a damping coefficient, c, of $0\,kg\,m^2\,rad^{-2}\,s^{-1}$), 1.0 J would contribute in different proportions to the total elastic energy thought to be available in the caudal region of three other dolphin species: 3 % for *Lagenorhynchus oliquidens* (34.06 J total), 7 % for *Tursiops truncatus* (13.46 J total) and 39 % for *Sotalia guianensis* (2.55 J total) (Bennet *et al.* 1987; Blickhan and Cheng, 1994). Anatomical data for *Delphinus delphis* are not available for the estimation of the total elastic energy. If elastic energy reduces the energy cost of locomotion in dolphins (see Blickhan and Cheng, 1994), any additional energy provided by the bending backbone would assist in that function.

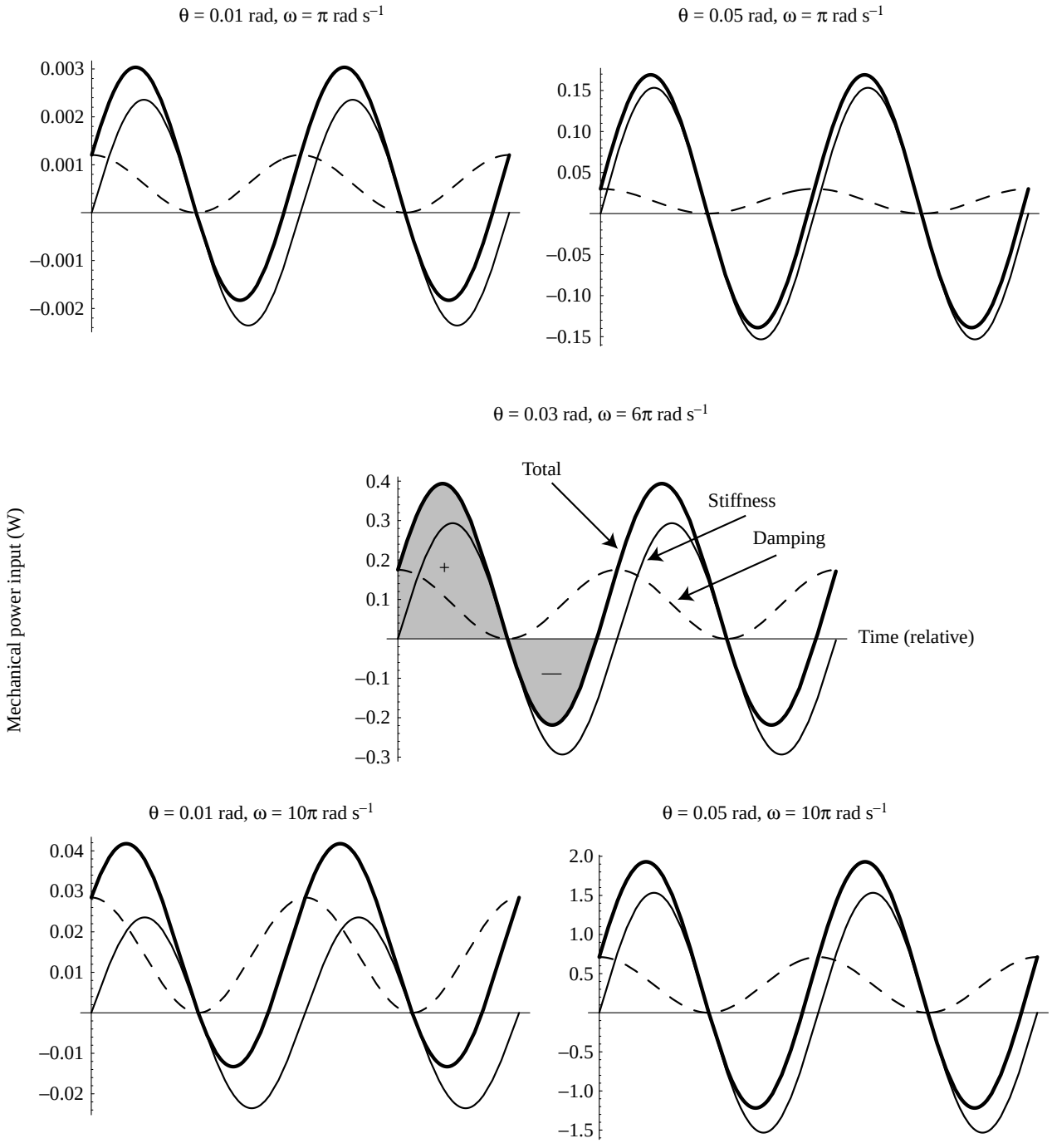

Fig. 10. Mechanical power needed to bend the caudal 7/8 intervertebral joint dynamically. Over the range of bending amplitudes (θ, rad) and frequencies (ω, rad s^{-1}) that include the physiological range in bottlenose dolphins (see Materials and methods), the interaction of non-linear stiffness and damping generates a range of mechanical behaviors. See Discussion for power calculations. One complete bending cycle for the joint (straight – maximum extension – straight – maximum flexion – straight) is represented in each graph (note that there is one power cycle for each *half*-cycle of vertebral bending). Bending amplitude increases in the graphs from left to right; bending frequency increases in the graphs from top to bottom. As represented on the middle graph, the total instantaneous power (thick solid line) required to bend the joint is the sum of the power due to the stiffness (thin solid line) and damping (dashed line) moments. The area under the curves (shaded) is the mechanical work done by the external bending source. Positive work is that needed from the external source; negative work is that returned in elastic recoil. The ratio of the negative to positive work is the resilience. Note that the power required to overcome the damping moment is always positive; thus, damping reduces the negative work returned during recoil. The relative influence of damping varies with different bending conditions.

Given this range of dynamic mechanical behavior (Fig. 10), how might the function of the caudal vertebral column differ with different swimming behaviors? For example, during steady swimming, dolphins increase speed by increasing tailbeat frequency (Fish, 1993). While little power is required to bend the vertebral column when using high-frequency, low-amplitude tailbeats, the proportion of energy recovered in the form of elastic recoil is also very low (approximately 20 %, see Fig. 7B). Thus, under these conditions, the vertebral column appears to act like a shock-absorber, not a spring. When using large-amplitude tailbeats, as might occur during accelerations, dolphins benefit from more energy return in the form of elastic recoil (approximately 50 %), but also require higher power output (2 W maximal) to bend the vertebral column at the fastest frequencies.

The resilience values of the dolphin intervertebral joints are lower than those reported for blue marlin (greater than 90 %; Long, 1992) and for a number of terrestrial mammals (65–75 % for lumbar joints in extension; Gal, 1993*b*). Why do dolphins possess a stiff but non-resilient vertebral column? The relatively low resilience of the dolphin intervertebral joints may provide dynamic stability to the column. That is, the joints may act to dissipate energy to prevent harmful break-away oscillations that may occur at frequencies near structural resonance (Meyhofer and Daniel, 1990). Alternatively, low resilience may simply be a consequence of increased vertebral flexibility. Gal (1993*b*) demonstrated that the lumbar intervertebral joints of tigers, jaguars and seals were less resilient (36–41 %) in flexion than those of monkeys or wallabies (65–67 %). Large cats and seals display great vertebral flexibility (e.g. Hildebrand, 1959; King, 1983).

The dynamic mechanical properties of dolphin intervertebral joints suggest that only at large bending amplitudes does the vertebral column store and release appreciable elastic strain energy. At lower amplitudes, the column dissipates strain energy with functional consequences, it is fair to say, that we do not yet completely understand.

Our results suggest that the pattern of body deformation observed in swimming dolphins is, in part, controlled by the mechanical behavior and morphology of the vertebral column. Clearly, these data are insufficient to explain dolphin swimming behavior completely. Factors that affect the pattern of whole-body deformation during swimming in vertebrates include (1) the mechanical properties of the axial skeleton (e.g. Long, 1992, 1995; Gal, 1993*a*,*b*; Bennett *et al*. 1987; Hebrank *et al.* 1990), (2) force production and distribution of the swimming muscles (e.g. Arkowitz and Rommel, 1985; Bennett *et al.* 1987; Blight, 1977; Long *et al.* 1994; Pabst, 1990, 1993; Rome *et al.* 1993; Wainwright, 1983; Westneat *et al.* 1993), (3) the mechanical properties of other body tissues that are deformed during swimming (i.e. fins, flukes, skin, subdermal sheaths) (Alexander, 1987; Fish and Hui, 1991; Pabst, 1996; Wainwright *et al.* 1978; Brainerd, 1994), and (4) interactions between the body and its fluid environment (Blight, 1977; Daniel and Webb, 1987; Fish, 1993; Gray, 1936; Lang, 1975; Lighthill, 1969; Vogel, 1994). Integrating data at all these levels is required to fully understand the mechanics of swimming in any vertebrate.

The authors wish to thank the following people for their contributions: Paul Bornemann, John Gosline, Ted Grand, Jim Mead, Charlie Potter, Butch Rommel, Meg Ronsheim, Steve Vogel and Steve Wainwright. This project was made possible through a cooperative agreement between the National Marine Fisheries Service and the Smithsonian Institution. J.H.L. and W.R.S. were supported by grant N000149310594 from the Office of Naval Research. D.A.P. and W.A.M. were supported by grant N000149310751 from the Office of Naval Research.

References

ALEXANDER, R. MCN. (1987). Bending of cylindrical animals with helical fibres in their skin or cuticle. *J. theor. Biol.* **124**, 97–110.

ALEXANDER, R. MCN., DIMERY, N. J. AND KER, R. F. (1985). Elastic structures in the back and their role in galloping in some mammals. *J. Zool., Lond.* **207**, 467–482.

ARKOWITZ, R. AND ROMMEL, S. A. (1985). Force and bending moment of the caudal muscles in the shortfin pilot whale. *Mar. Mammal Sci.* **1**, 203–209.

BENNETT, M. B., KER, R. F. AND ALEXANDER, R. MCN. (1987). Elastic properties of structures in the tails of cetaceans (*Phocoena* and *Lagenorhynchus*) and their effect on the energy cost of swimming. *J. Zool., Lond.* **211**, 177–192.

BLICKHAN, R. AND CHENG, J.-Y. (1994). Energy storage by elastic mechanisms in the tail of large swimmers – a re-evaluation. *J. theor. Biol.* **168**, 315–321.

BLIGHT, A. R. (1977). The muscular control of vertebrate swimming movements. *Biol. Rev.* **52**, 181–218.

BRAINERD, E. L. (1994). Mechanical design of polypterid fish integument for energy storage during recoil aspiration. *J. Zool., Lond.* **232**, 7–19.

DANIEL, T. L. AND WEBB, P. W. (1987). Physical determinants of locomotion. In *Comparative Physiology: Life in Water and on Land* (ed. P. Dejours, L. Bolis, C. R. Taylor and E. R. Weibel), pp. 343–369. New York: Liviana Press.

DEN HARTOG, J. P. (1949). *Strength of Materials.* London: Constable & Co. Ltd.

DEN HARTOG, J. P. (1956). *Mechanical Vibrations*, fourth edition. New York: McGraw-Hill.

DENNY, M. W. (1988). *Biology and the Mechanics of the Wave-Swept Environment.* Princeton: Princeton University Press.

DIAL, K. P. (1992). Activity patterns of the wing muscles of the pigeon (*Columbia livia*) during different modes of flight. *J. exp. Zool.* **262**, 357–373.

FISH, F. E. (1993). Power output and propulsive efficiency of swimming bottlenose dolphins (*Tursiops truncatus*). *J. exp. Biol.* **185**, 179–193.

FISH, F. E. AND HUI, C. A. (1991). Dolphin swimming – a review. *Mammal Rev.* **21**, 181–195.

GAL, J. (1992). Spinal flexion and locomotor energetics in kangaroo, monkey and tiger. *Can. J. Zool.* **70**, 2444–2451.

GAL, J. (1993*a*). Mammalian spinal biomechanics. I. Static and dynamic mechanical properties of intact intervertebral joints. *J. exp. Biol.* **174**, 247–280.

GAL, J. (1993*b*). Mammalian spinal biomechanics. II. Intervertebral

lesion experiments and mechanisms of bending resistance. *J. exp. Biol.* **174**, 281–297.

GINGERICH, P. D., RAZA, S. M., ARIF, M., ANWAR, M. AND ZHOU, X. (1994). New whale from the eocene of Pakistan and the origin of cetacean swimming. *Nature* **368**, 844–847.

GRAY, J. (1936). Studies in animal locomotion. VI. The propulsive powers of the dolphin. *J. exp. Biol.* **13**, 192–199.

HEBRANK, J. H., HEBRANK, M. R., LONG, J. H., JR, BLOCK, B. A. AND WAINWRIGHT, S. A. (1990). Backbone mechanics of the blue marlin *Makaira nigricans* (Pisces, Istiophoridae). *J. exp. Biol.* **148**, 449–459.

HEBRANK, M. R. (1982). Mechanical properties of fish backbones in lateral bending and in tension. *J. Biomech.* **15**, 85–89.

HILDEBRAND, M. (1959). Motions of the running cheetah and horse. *J. Mammal.* **40**, 481–495.

KING, J. E. (1983). *Seals of the World*, second edition. New York: Comstock Publishing Associates.

LANG, T. G. (1975). Speed, power and drag measurements of dolphins and porpoises. In *Swimming and Flying in Nature* (ed. T. Y. Wu, C. J. Brokaw and C. Brennen), pp. 553–571. New York: Plenum Press.

LIGHTHILL, M. J. (1969). Hydromechanics of aquatic animal propulsion. *A. Rev. Fluid Mech.* **1**, 413–446.

LONG, J. H., JR (1992). Stiffness and damping forces in the intervertebral joints of blue marlin (*Makaira nigricans*). *J. exp. Biol.* **162**, 131–155.

LONG, J. H., JR (1995). Morphology, mechanics and locomotion: the relation between the notochord and swimming motions in sturgeon. *Env. Biol. Fishes* **44**, 199–211.

LONG, J. H., JR, MCHENRY, M. J. AND BOETTICHER, N. C. (1994). Undulatory swimming: how traveling waves are produced and modulated in sunfish (*Lepomis gibbosus*). *J. exp. Biol.* **192**, 129–145.

MCHENRY, M. J., PELL, C. A. AND LONG, J. H., JR (1995). Mechanical control of swimming speed: stiffness and axial wave form in undulating fish models. *J. exp. Biol.* **198**, 2293–2305.

MEYERHOFER, E. AND DANIEL, T. (1990). Dynamic mechanical properties of extensor muscle cells of the shrimp *Pandalus danae*: cell design for escape locomotion. *J. exp. Biol.* **151**, 435–452.

PABST, D. A. (1990). Axial muscles and connective tissues of the bottlenose dolphin. In *The Bottlenose Dolphin* (ed. S. Leatherwood and R. R. Reeves), pp. 51–67. San Diego, London: Academic Press.

PABST, D. A. (1993). Intramuscular morphology and tendon geometry of the epaxial swimming muscles of dolphins. *J. Zool., Lond.* **230**, 159–176.

PABST, D. A. (1996). Morphology of the subdermal connective tissue sheath of dolphins: a new fibre-wound, thin-walled pressurized cylinder model for swimming vertebrates. *J. Zool., Lond.* **238**, 35–52.

PANTIN, C. F. A. (1964). *Notes on Microscopical Technique for Zoologists*. Cambridge: Cambridge University Press.

PARRY, D. A. (1949). The swimming of whales and a discussion of Gray's paradox. *J. exp. Biol.* **26**, 24–34.

ROME, L. C., SWANK, D. AND CORDA, D. (1993). How fish power swimming. *Science* **261**, 340–343.

ROMMEL, S. A. (1990). Osteology of the bottlenose dolphin. In *The Bottlenose Dolphin* (ed. S. Leatherwood and R. R. Reeves), pp. 29–49. San Diego, London: Academic Press.

SAS INSTITUTE INC. (1985). *SAS User's Guide: Statistics*, version 5. Cary, NC: SAS Institute, Inc.

SHIRAZI-ADL, A. (1989). On the fibre composite material models of disc annulus – comparison of predicted stresses. *J. Biomech.* **22**, 357–365.

SLIJPER, E. J. (1936). Die Cetaceen Vergleichend-anatomisch und Systematisch. *Capita Zool.* **7**, 1–600.

SLIJPER, E. J. (1946). Comparative biologic–anatomical investigations on the vertebral column and spinal musculature of mammals. *Verh. K. Ned. Akad. Wet. Afd. Natuurk. Sect. 2* **42**, 1–128.

SOKAL, R. R. AND ROHLF, F. J. (1981). *Biometry*, second edition. New York: W. H. Freeman & Co.

TENCER, A. F., AHMED, A. M. AND BURKE, D. L. (1982). Some static mechanical properties of the lumbar joint, intact and injured. *J. biomech. Eng.* **104**, 193–201.

THEWISSEN, J. G. M., HUSSAIN, S. T. AND ARIF, M. (1994). Fossil evidence for the origin of aquatic locomotion in archaeocete whales. *Science* **263**, 210–212.

VIDELER, J. AND KAMERMANS, P. (1985). Differences between upstroke and downstroke in swimming dolphins. *J. exp. Biol.* **119**, 265–274.

VOGEL, S. (1994). *Life in Moving Fluids: The Physical Biology of Flow*, second edition. Princeton: Princeton University Press.

WAINWRIGHT, S. A. (1983). To bend a fish. In *Fish Biomechanics* (ed. P. W. Webb and D. Weihs), pp. 68–91. New York: Praeger.

WAINWRIGHT, S. A., BIGGS, W. D., CURREY, J. D. AND GOSLINE, J. M. (1976). *Mechanical Design in Organisms*. New York: John Wiley and Sons.

WAINWRIGHT, S. A., ORTON, L. S. AND PABST, D. A. (1987). Analysis of skin strain and swimming kinematics of an unrestrained dolphin from highspeed films. *NOSC Final Report, Contract No. N66001-86-M-7855*.

WAINWRIGHT, S. A., VOSBURGH, F. AND HEBRANK, J. H. (1978). Shark skin: function in locomotion. *Science* **202**, 747–749.

WESTNEAT, M. W., HOESE, W., PELL, C. A. AND WAINWRIGHT, S. A. (1993). The horizontal septum: mechanics of force transfer in locomotion of scombrid fishes (Scombridae, Perciformes). *J. Morph.* **217**, 183–204.

WILKINSON, L. (1989). *SYSTAT: The System for Statistics*. Evanston, IL: SYSTAT, Inc.